Liquid Motions in Nonaxisymmetric, Partially Filled Containers Rotating at Zero Gravity

D. Weihs* and F. T. Dodge†
Southwest Research Institute, San Antonio, Texas 78228

Sloshing and internal wave motions of liquid in rotating wedge-shaped tanks are studied. The tank cross section is composed of a cylindrical annulus with sidewalls that are radial rays. The axis of rotation is the axis of the cylinder. The liquid is inviscid and incompressible. Closed-form solutions are obtained for the full three-dimensional flowfield, as well as for the limiting cases of axisymmetric and two-dimensional cylindrical containers. Two kinds of oscillating motions are found. For motions that are completely internal (i.e., have no oscillation of the free surface), infinite families of discrete frequencies were predicted, with all frequencies being less than twice the rotation frequency. For oscillations with frequencies greater than twice the rotation frequency, each harmonic supplied one or two characteristic sloshing modes (i.e., having an oscillation of the free surface), depending upon the geometrical parameters. These solutions should prove useful in validating approximate theories for situations in which an exact analysis is not possible.

Nomenclature

A	= outer tank radius
A_i	= coefficients of Bessel functions in the various solutions ($i = 1, \ldots, 6$)
B	= nondimensional inner tank radius
H	= tank height
I	= modified Bessel function of the first kind
J	= Bessel function of the first kind
K	= modified Bessel function of the second kind
k, l	= nondimensional wave numbers in the circumferential and axial directions, respectively
m	= index, see Eq. (30)
n	= nondimensional temporal wave number
P	= radial pressure function, Eq. (29)
p	= pressure
q	= index, see Eq. (32)
r	= radial direction
s	= quantity defining tank sector angle (see Fig. 1)
U, V, W	= radial velocity functions, see Eqs. (26–28)
u, v, w	= velocity components in the radial, circumferential, and axial directions, respectively
X	= center of rotation (see Fig. 1)
Y	= Bessel function of the second kind
z	= axial coordinate
α	= tank fill ratio
δ	= free surface perturbation
Δ	= amplitude of free surface perturbation
ϵ	= nondimensional thickness of liquid layer, Eq. (56)
ζ	= quantity defining tank height as a multiple of outer radius (Fig. 1)
θ	= circumferential coordinate
Θ	= tank sector angle
λ	= Bessel function parameter [$\equiv (4-n^2)/n$]
ρ	= liquid density
σ	= zeros of Eq. (63)
Ω	= spinning frequency

Subscripts

a	= secondary flows
d	= index
k	= Bessel function order

Received April 23,1990; revision received Oct. 24, 1990; second revision received Feb. 28, 1991; accepted for publication March 8, 1991.

*Consultant; currently Professor of Aerospace Engineering, Technion, Haifa, Israel.

†Institute Engineer, Division of Mechanical and Fluids Engineering.

I. Introduction

STABILIZATION of spacecraft is often accomplished by spinning, a technique that is also useful for reducing solar heating effects. Although the spacecraft is rotated around one of its axes of symmetry, any liquid container onboard spins, in most cases, about an axis that is different from any of its own symmetry axes; usually, the spin axis lies outside of the tank. This off-axis rotation can result in large liquid motions relative to the tank walls. One well-known example of the energy that can be dissipated by such motions is the growth of nutation when the craft is spun about its minor moment of inertia. If the growth is unchecked, the nutation results in a tumbling motion around the major moment of inertia axis, sometimes referred to as a flat spin.[1,2] When this occurs for spacecraft in low Earth orbits, the useful life of the satellite is usually over, as the antennae are no longer pointed in the right direction and communication with the satellite is sporadic, at best. Also, the increased drag obtained due to the broadside motion can result in slowing the vehicle, even leading to its loss. Satellites in higher orbits, where aerodynamic drag is no longer a consideration, can suffer from loss of control. The energy required to counter these tendencies is, in many cases, the dominant factor in determining the useful life of orbiting spacecraft.

The bulk liquid motions observed in tanks include unsteady spin-up and spin-down effects, and "steady" motions that occur when the spinning has persisted at a given frequency Ω for time periods long enough for the spin-up transients to have vanished. These steady flowfields include, in addition to the basic solid-body rotation, various secondary periodic motions such as internal waves and sloshing (when there is a free surface). For a spinning spacecraft, liquid oscillations having a frequency less than the spin rate are the main source of concern since they can resonate with the nutation motion. Understanding the mechanisms causing such liquid motions are of great significance to the efficient design of orbiters and other spacecraft, and much effort has been spent in analyzing the liquid motion effects.[3,4] However, the calculations and

codes available now do not accurately predict the observed internal waves[5] because of a lack of basic theoretical models to describe the various modes.

The motions resulting from precession of a liquid-filled top were analyzed by Stewartson,[6,7] and approximate models in which the vorticity is averaged over the liquid volume have been adapted from these analyses.[8] The approximate models, while used as the basis for computational models, have been shown to result in fictitious instabilities,[9] strengthening the need for better models. The present study attempts to develop such a model, by examining an idealized configuration but one which is still of practical importance.[10,11] We look at the motions induced in the fluid in a partially filled, noncircular cylindrical tank rotating at speed Ω around an axis, which is parallel to, but displaced from, the cylinder axis. To make an exact analysis possible, the tank cross section is chosen to be a circular, annular section, so that the sidewalls are radial rays and the top and bottom are parallel to each other and perpendicular to the axis of rotation, as shown in Fig. 1. The tank is in an environment of negligible gravity and has been spinning for a long time, so that the only body forces are the result of steady centripetal accelerations. The problem is thus an idealization of a circular cylindrical tank with a diameter roughly equal to the distance between the radial walls situated off-center in a spinning spacecraft. It includes most of the characteristics of existing tanks. The model does not consider inclinations of the spinning axis, thus separating out the effects of nutation as treated by Stewartson.

The present paper deals with partially filled tanks, so that free surfaces are present. Neglecting surface tension and contact-angle effects, the steady, undisturbed free surface forms a circular arc in cross section, centered on the vehicle axis of rotation. This configuration allows for geostrophic and internal wave motions, thus enabling comparison with the "homogeneous vortex" models mentioned previously.[8,9] The solution of the general case is rather complicated, with dependence on two geometric parameters and the liquid depth, and it exhibits azimuthal, axial, and mixed harmonic oscillations. Some simpler two-dimensional cases are shown for clarity. These are the depth-independent and axisymmetric wave solutions, respectively.

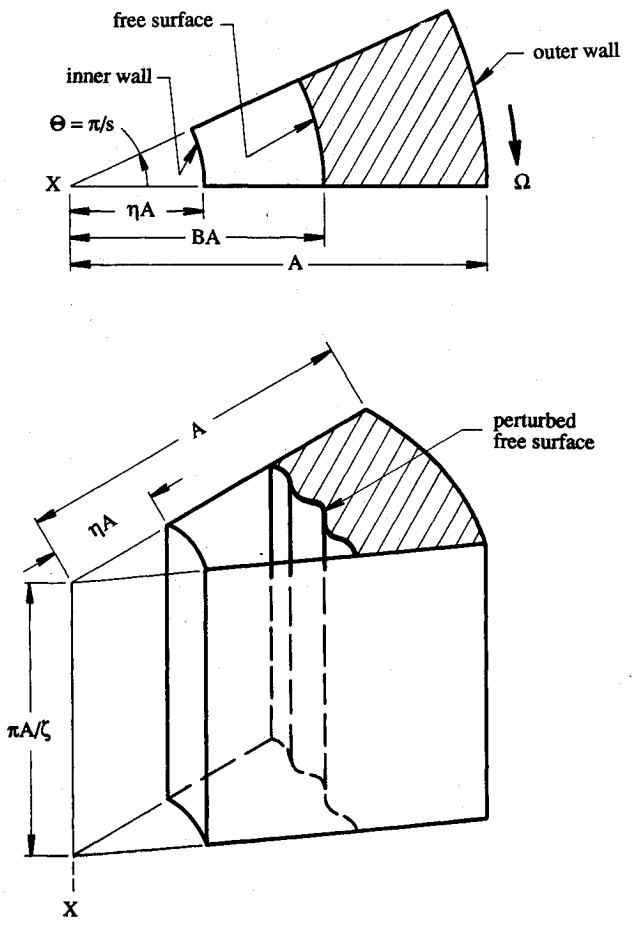

Fig. 1 Schematic of tank configuration; shaded area indicates liquid.

II. Analysis

The fluid system treated is bounded by a solid tank with cross section in the shape of a circular sector. The outer radius of the tank is A, the inner radius ηA, its height $H = \pi A/\zeta$, and the included angle of the sector is $\Theta = \pi/s$ (see Fig. 1). The container is partially filled with an inviscid, incompressible liquid of density ρ.

The container is considered to have been rotating for a long time at speed Ω, so that spin-up effects have subsided.[12] The axis of rotation is the origin of the circular arcs produced by the inner and outer wall of the tank. The free-surface equilibrium position, except for small zones at contact with the tank walls, can therefore be considered as an arc of a concentric circle of radius BA, where $\eta < B < 1$. B is obtained from the fill ratio α of the tank by

$$B^2 = (1 - \alpha) \tag{1}$$

We write out the equations of motion in a cylindrical coordinate system rotating at speed Ω and centered on the axis of rotation[13]:

$$\frac{\partial u}{\partial t} + u\frac{\partial u}{\partial r} + \frac{v}{r}\frac{\partial u}{\partial \theta} + w\frac{\partial u}{\partial z} - \frac{v^2}{r} - 2\Omega v - \Omega^2 r = \frac{1}{\rho}\frac{\partial p}{\partial r} \tag{2}$$

$$\frac{\partial v}{\partial t} + u\frac{\partial v}{\partial r} + \frac{v}{r}\frac{\partial v}{\partial \theta} + w\frac{\partial v}{\partial z} + \frac{uv}{r} + 2\Omega u = -\frac{1}{r\rho}\frac{\partial p}{\partial \theta} \tag{3}$$

$$\frac{\partial w}{\partial t} + u\frac{\partial w}{\partial r} + \frac{v}{r}\frac{\partial w}{\partial \theta} + w\frac{\partial w}{\partial z} = -\frac{1}{\rho}\frac{\partial p}{\partial z} \tag{4}$$

$$\frac{1}{r}\frac{\partial}{\partial r}(ru) + \frac{1}{r}\frac{\partial v}{\partial \theta} + \frac{\partial w}{\partial z} = 0 \tag{5}$$

Here u, v, w are the velocity components in the radial r, circumferential θ, and axial z directions, respectively. We now nondimensionalize these equations by dividing lengths by A, speeds by ΩA, time by Ω^{-1}, and p by $\rho(\Omega A)^2$. All variables will henceforth be nondimensional, and the equations now read, respectively,

$$\frac{\partial u}{\partial t} + u\frac{\partial u}{\partial r} + \frac{v}{r}\frac{\partial u}{\partial \theta} + w\frac{\partial u}{\partial z} - \frac{v^2}{r} - 2v - r = -\frac{\partial p}{\partial r} \tag{6}$$

$$\frac{\partial v}{\partial t} + u\frac{\partial v}{\partial r} + \frac{v}{r}\frac{\partial v}{\partial \theta} + w\frac{\partial v}{\partial z} + \frac{uv}{r} + 2u = -\frac{1}{r}\frac{\partial p}{\partial \theta} \tag{7}$$

$$\frac{\partial w}{\partial t} + u\frac{\partial w}{\partial r} + \frac{v}{r}\frac{\partial w}{\partial \theta} + w\frac{\partial w}{\partial z} = -\frac{\partial p}{\partial z} \tag{8}$$

$$\frac{\partial u}{\partial r} + \frac{u}{r} + \frac{1}{r}\frac{\partial v}{\partial \theta} + \frac{\partial w}{\partial z} = 0 \tag{9}$$

The steady flowfield will be a solid-body rotation. We now look for small secondary perturbations, as an indication of disturbances that might grow into larger streaming motions. These could be either internal waves[13] or free-surface, sloshing waves.[3]

Looking for a secondary flow, we take the secondary pressure field p_a to be small relative to the solid-body rotation. Thus,

$$p = p_0 + p_a \tag{10}$$

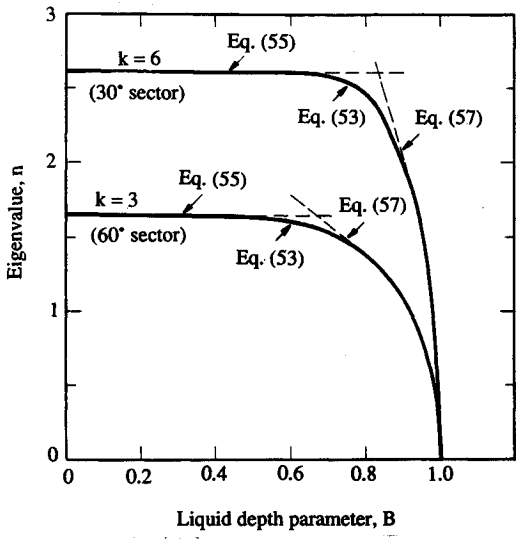

Fig. 2 Eigenvalues for long ($l = 0$) tanks of 30- and 60-deg sector angles, as a function of liquid depth. The broken lines indicate the deep-layer and thin-layer approximations.

$$u = u_a \tag{11}$$

$$v = v_a, \qquad w = w_a \tag{12}$$

where all of the quantities subscripted a represent secondary flows and are $\ll 1$. For the basic case of no secondary motions, $u = v = w = 0$, and Eqs. (7–9) are trivially satisfied. Equation (6) results in

$$-r = -\frac{\partial p_0}{\partial r} \tag{13}$$

Thus, for the first-order equations, neglecting squares and products of small quantities and requiring $r \neq 0$ (i.e., $B \neq 0$), we obtain from Eqs. (6–9)

$$\frac{\partial u_a}{\partial t} - 2v_a = -\frac{\partial p_a}{\partial r} \tag{14}$$

$$\frac{\partial v_a}{\partial t} + 2u_a = -\frac{1}{r}\frac{\partial p_a}{\partial \theta} \tag{15}$$

$$\frac{\partial w_a}{\partial t} = -\frac{\partial p_a}{\partial z} \tag{16}$$

$$\frac{\partial u_a}{\partial r} + \frac{u_a}{r} + \frac{1}{r}\frac{\partial v_a}{\partial \theta} + \frac{\partial w_a}{\partial z} = 0 \tag{17}$$

The boundary conditions for the secondary flowfield, Eqs. (14–17), at the solid boundaries are

$$u_a = 0 \qquad \text{at } r = 1 \qquad \text{(the outer wall)} \tag{18}$$

$$v_a = 0 \qquad \text{at } \theta = \pm\Theta/2 \qquad \text{(side walls, } \Theta < \pi\text{)} \tag{19}$$

$$w_a = 0 \qquad \text{at } z = \pm\pi/2\zeta \qquad \text{(top and bottom walls)} \tag{20}$$

The free surface supplies a second condition required for the radial component of velocity, as well as the condition required for the pressure. The free surface can be written as

$$r = B + \delta(\theta, z, t) \tag{21}$$

We can, without loss of generality, consider the free-surface perturbation to be periodic in time and in the θ and z directions. In keeping with the small-perturbation assumption, then

$$\delta = \Delta e^{i(k\theta + lz + nt)}, \qquad (\Delta \ll B) \tag{22}$$

The radial velocity u_B at the interface can then be written as

$$u_B = \frac{\partial \delta}{\partial t} + v_B\frac{\partial \delta}{\partial \theta} + w_B\frac{\partial \delta}{\partial z} \approx \frac{\partial \delta}{\partial t} \tag{23}$$

where the second and third terms on the right-hand side of Eq. (23) are neglected, being products of two small quantities. From Eq. (22), the condition for the radial velocity of the free surface is then

$$u = in\Delta e^{i(k\theta + lz + nt)} \qquad \text{at } r = B \tag{24}$$

The pressure at the free surface is constant, and can be taken as zero. Then, for small radial excursions δ, the dimensional pressure $p = \rho\Omega^2(r^2 - B^2 + p_a)/2$ at the free surface reduces to

$$p_a + 2B\delta = 0 \qquad \text{at } r = B \tag{25}$$

Equations (24) and (25) should both be evaluated at the instantaneous free surface, but again we neglect products of small quantities to apply them at B. From Eqs. (24) and (25), periodic solutions are indicated for the velocities and pressures, in the form

$$u_a(r, \theta, z, t) = U(r)e^{i(k\theta + lz + nt)} \tag{26}$$

$$v_a(r, \theta, z, t) = V(r)e^{i(k\theta + lz + nt)} \tag{27}$$

$$w_a(r, \theta, z, t) = W(r)e^{i(k\theta + lz + nt)} \tag{28}$$

$$p_a(r, \theta, z, t) = P(r)e^{i(k\theta + lz + nt)} \tag{29}$$

Equations (19) and (20) immediately relate the unknowns k and l with the tank geometry. From Eqs. (19) and (27), with $\Theta \equiv \pi/s$, $(s > 1/2)$, the real part of Eq. (27) vanishes when

$$\pm\frac{k\pi}{2s} = \frac{\pi}{2}(2m + 1), \qquad m = 0, 1, 2, \ldots \tag{30}$$

or

$$k = \pm(2m + 1)s, \qquad m = 0, 1, 2, \ldots \tag{31}$$

Similarly, from Eqs. (20) and (28),

$$l = \pm(2q + 1)\zeta, \qquad q = 0, 1, 2, \ldots \tag{32}$$

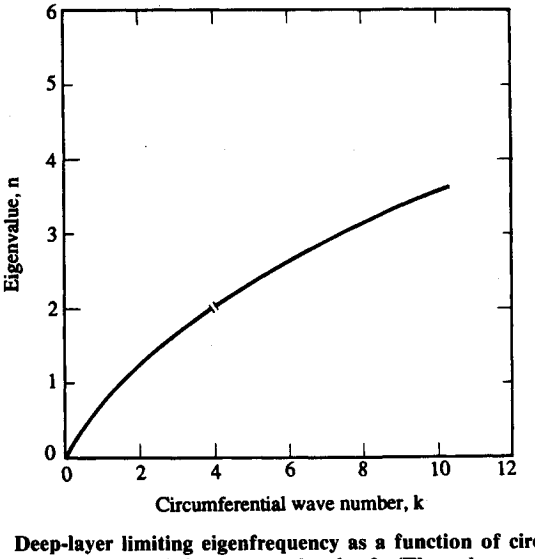

Fig. 3 Deep-layer limiting eigenfrequency as a function of circumferential wave number k for long tanks, $l = 0$. (The value $n = 2$ is singular.)

These substitutions leave us with a one-dimensional, time-dependent problem, where n and the various functions of r still need to be established. Substituting Eqs. (26–29) into Eqs. (14–17), we obtain

$$inU - 2V = -P' \tag{33}$$

$$inV + 2U = -\frac{ik}{r}P \tag{34}$$

$$inW = -ilP \tag{35}$$

$$U' + \frac{U}{r} + \frac{ikV}{r} + ilW = 0 \tag{36}$$

We obtain from Eqs. (33) and (34)

$$U = \frac{-i}{4-n^2}\left(\frac{2k}{r}P + nP'\right) \tag{37}$$

$$V = \frac{1}{4-n^2}\left(\frac{nk}{r}P + 2P'\right) \tag{38}$$

From Eqs. (35–38) we obtain an equation for P, which, after some manipulations, reads

$$r^2P'' + rP' + \left[r^2\frac{l^2}{n^2}(4-n^2) - k^2\right]P = 0 \tag{39}$$

This is a variant of Bessel's equation, with solutions

$$P = A_1J_k\left(\frac{l}{n}\sqrt{4-n^2}r\right) + A_2Y_k\left(\frac{l}{n}\sqrt{4-n^2}r\right) \tag{40}$$

Both kinds of Bessel's functions occur in Eq. (40), since both bounds for r are finite. The values for k and l are obtained from Eqs. (31) and (32), so that the remaining three boundary conditions establish A_1, A_2, and n. The value $n = 2$ is a critical point [cf. Eq. (39)]. This is reflected in the fact that for $n > 2$, the argument becomes imaginary, so that for real arguments to be kept, the modified Bessel functions I_k and K_k appear in Eq. (40) and its sequels.

Using various identities relating to Bessel's functions and their derivatives,[14] we obtain from Eq. (37), using Eq. (40)

$$U = \frac{i}{n^2-4}\left[A_1\lambda\left(\frac{2+n}{2}J_{k-1}(\lambda r) + \frac{2+n}{2}J_{k+1}(\lambda r)\right) + A_2\lambda\left(\frac{2+n}{2}Y_{k-1}(\lambda r) + \frac{2-n}{2}Y_{k+1}(\lambda r)\right)\right] \tag{41}$$

and from Eq. (18)

$$\frac{A_2}{A_1} = -\frac{(2+n)J_{k+1}(\lambda) + (2-n)J_{k+1}(\lambda)}{(2+n)Y_{k+1}(\lambda) + (2-n)Y_{k+1}(\lambda)} \tag{42}$$

where

$$\lambda = \frac{l}{n}\sqrt{4-n^2} \tag{43}$$

Next, we substitute Eq. (40) into condition (25):

$$A_1\left[J_k(\lambda B) + \frac{A_2}{A_1}Y_k(\lambda B)\right] + 2B\Delta = 0 \tag{44}$$

so that, with Eq. (42),

$$A_1 = -(2B\Delta)\Big/\left[J_k(\lambda B) - \frac{(2+n)J_{k-1}(\lambda) + (2-n)J_{k+1}(\lambda)}{(2+n)Y_{k-1}(\lambda) + (2-n)Y_{k+1}(\lambda)}Y_k(\lambda B)\right] \tag{45}$$

To obtain permissible frequencies n, we return to Eqs. (23) and (24), from which, after substituting into Eq. (41) and further manipulation,

$$n(4-n^2) = \frac{(2+n)J_{k-1}(\lambda B) + (2-n)J_{k+1}(\lambda B) + (A_2/A_1)[(2+n)Y_{k-1}(\lambda B) + (2-n)Y_{k+1}(\lambda B)]}{J_k(\lambda B) + (A_2/A_1)Y_k(\lambda B)} \tag{46}$$

where Δ cancels out; as is to be expected, the frequencies do not depend on the arbitrary (small) amplitude. These permissible frequencies can now be calculated from Eq. (46) using Eq. (42).

Returning to Eq. (44), we see that when the term in brackets vanishes, surface deflections do not occur. This implies that only internal waves (i.e., motions limited to the fluid interior, without surface deflections) are obtained when

$$A_1\left[J_k(\lambda B) + \frac{A_2}{A_1}Y_k(\lambda B)\right] = 0 \tag{47}$$

This result includes, but is not limited to, the case of a rigid wall at $r = B$, such as obtained when the tank is completely full. Although Eq. (47) is not a rigorous proof of the existence of internal waves at these frequencies, there is ample experimental evidence of such modes,[5] usually denoted as inertial waves. A proof would require a full nonlinear analysis, which is beyond the scope of this analysis.

The singular points of Eq. (46) are the roots of Eq. (47). Thus, nontrivial solutions of Eq. (46) will result in sloshing modes, here defined as causing deflections of the free surface, while Eq. (47) characterizes the internal modes.

III. Results

Equations (46) and (47) provide the eigenfrequencies for sloshing and inertial waves, respectively, for linearized disturbances. Once these frequencies are available, the pressure distribution and velocity fields are easily obtained from Eqs. (40), (41), and equivalent equations for the circumferential and axial velocity components. Although these collectively are an exact analytical solution, the complexity of the various expressions preclude any simple closed-form dependencies, except for the general conclusions about the different modes with or without free-surface perturbation. Before going on to calculate specific examples, we examine some special cases, which allow for simplification of the results.

A. Two-Dimensional Motions

For an infinitely long cylindrical container, there is a possibility of two-dimensional flow with $l = 0$. This will probably be a good approximation for highly elongated tanks. Equation (35) vanishes identically for this case, and Eq. (39) turns into

$$r^2P'' + rP' - k^2P = 0 \tag{48}$$

The general solution here is

$$P = A_3 r^k + A_4 r^{-k} \tag{49}$$

and, instead of Eq. (41), we have

$$U = -\frac{ik}{4-n^2}[(2+n)A_3 r^{k-1} + (2-n)A_4 r^{-k-1}] \tag{50}$$

The boundary conditions of Eqs. (18), (19), (23), and (25) are still valid, with the only difference being that the z dependence has vanished. From Eq. (18),

$$A_4 = -A_3\frac{2+n}{2-n} \tag{51}$$

while from Eq. (23), in analogy to Eq. (45),

$$A_3 = \frac{\Delta n(n-2)}{k(B^{k-1} - B^{-k-1})} \tag{52}$$

Applying Eq. (25), we obtain an equation for n, after some manipulations, as

$$(n^2 - 2n + 2k)B^k + (n^2 + 2n - 2k)B^{-k} = 0, \qquad n \neq 2 \tag{53}$$

Recalling that k is a doubly infinite series of solutions for any sector angle Θ [see Eq. (31)], we find that two-dimensional circumferential wave solutions are possible, but they all require free-surface perturbations.

Upon observing that $B < 1$ and that $k \geq 1$ for many realistic cases, one can simplify Eq. (53) further for the case where $B^k \ll B^{-k}$. This reduces Eq. (53) to a quadratic equation for n for each k, namely,

$$n^2 + 2n - 2k \approx 0 \tag{54}$$

or

$$n = -1 \pm \sqrt{1+2k} \tag{55}$$

Another limiting case of two-dimensional disturbances is obtained for very thin annular liquid layers, i.e., $B = 1 - \epsilon$, such that $\epsilon k \ll 1$. In this case, Eq. (53) can be approximated by

$$n^2 + 2k\epsilon n - 2k^2\epsilon = 0 \tag{56}$$

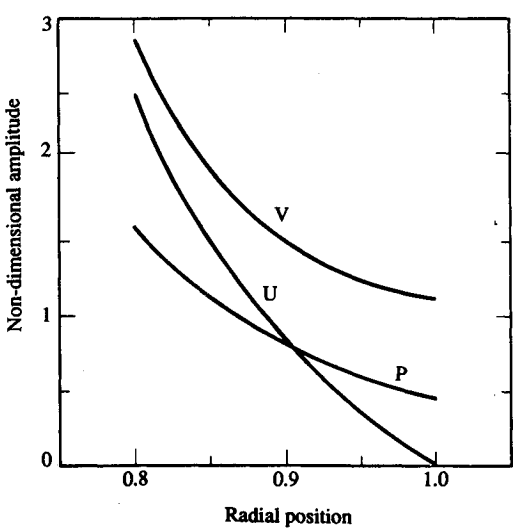

Fig. 4 Amplitude of radial U and circumferential V velocities and pressure P of the fundamental wave, $l = 0$ [Eqs. (58–60)], for a 30-deg sector tank with the free surface at $B = 0.8$.

Table 1 Nondimensional internal wave eigenfrequencies for a spinning annular liquid layer of finite height $\zeta = 6$ ($H = 0.524A$); $B = 0.8$

	Eigenfrequency number			
Wavelengths	1	2	3	4
0	0.860	0.464	0.314	0.237
1	1.64	1.16	0.861	0.695
2	1.84	1.53	1.24	1.025
3	1.91	1.71	1.48	1.282

or

$$n = -k\epsilon\left(1 \mp \sqrt{1+\frac{2}{\epsilon}}\right) \tag{57}$$

Quantitative results for the frequencies obtained for two-dimensional motions appear in Figs. 2 and 3. Figure 2 shows the lowest harmonic disturbance eigenfrequency n as a function of tank liquid depths, for $k = 3$ (sector angle 60 deg) and $k = 6$ (sector angle 30 deg) containers. The approximate solutions for deep- and shallow-liquid filling appear as broken lines while the complete solution [Eq. (53)] is the full line. It can be seen that when the free surface is at half of the external radius or less, the deep-liquid approximation is extremely accurate, while the shallow-layer solution fits layers of up to 10% depth very well. The disturbance frequency expected for a gradually emptying tank (as the satellite uses up its fuel) is seen to stay fixed at first, then drop rapidly as the remaining layer becomes thinner.

The limiting deep-liquid frequency is mapped for tanks of varying sector angle in Fig. 3. As the tank becomes narrower, the frequency goes up, asymptotically as the inverse square root of the angle.

Next, we write out the velocity components and the pressure. From Eqs. (50–52) and (26),

$$u_a = \frac{n\Delta}{B^{k-1} - B^{-k-1}}(r^{k-1} - r^{-k-1})\sin(k\theta + nt) \tag{58}$$

and, applying Eq. (33),

$$v_a = -\frac{n\Delta}{B^{k-1} - B^{-k-1}}(r^{k-1} + r^{-k-1})\cos(k\theta + nt) \tag{59}$$

$$p_a = -\frac{n\Delta}{k(B^{k-1} - B^{-k-1})}[(n-2)r^k + (n+2)r^{-k}]\cos(k\theta + nt) \tag{60}$$

The amplitudes of Eqs. (58–60) appear as a function of radial distance in Fig. 4, for a case $B = 0.8$, $\Theta = 30$ deg and frequency (from Fig. 3) $n = 2.477$.

A different two-dimensional example is obtained in the axisymmetric case. Here $\Theta = 2\pi$, i.e., the container has an annular form, and $k = 0$. This case can be solved by substituting $k = 0$ in Eqs. (37–39). Thus,

$$P = A_5 J_0\left(\frac{l}{n}\sqrt{4-n^2}\,r\right) + A_6 Y_0\left(\frac{l}{n}\sqrt{4-n^2}\,r\right) \tag{61}$$

Following steps similar to those in Sec. II, one arrives at values

$$\frac{A_6}{A_5} = -\frac{J_1(\lambda)}{Y_1(\lambda)}$$

where

$$\lambda = \frac{l}{n}\sqrt{4-n^2} \tag{62a}$$

$$A_5 = \Delta\frac{n}{l}\sqrt{4-n^2}\left(1\Big/\left[J_1(\lambda B) - \frac{J_1(\lambda)}{Y_1(\lambda)}Y_1(\lambda B)\right]\right) \tag{62b}$$

Thus, internal axisymmetric modes with no free-surface perturbations are obtained when

$$J_1(\lambda B)Y_1(\lambda) - J_1(\lambda)Y_1(\lambda B) = 0 \qquad (63)$$

The values of λ that satisfy Eq. (63) for given values of B are shown in Table 9.7 of Ref. 14. Defining the dth zero of Eq. (63) for given B as $\sigma_d(B)$, we have from Eq. (61)

$$\sigma_d(B) = \frac{l}{n}\sqrt{4-n^2}, \qquad n<2 \qquad (64)$$

For example, when $\zeta = 6$ (i.e., tank height is 0.524 of the outer wall radius) and $B = 0.8$, $\sigma_1(0.8) = 25.59$ and $n = 0.860$ for the fundamental wave number [$q = 0$, cf. Eq. (32)]; $\sigma_2(0.8) = 12.14$ and $n = 0.464$; and higher zeros give a series of descending frequencies. Higher wave number harmonies, ($q = 1, 2, \ldots$) also produce such motions; see Table 1. All frequencies are $n < 2$, as expected for internal waves, and from Table 1 there may be an indication of a nonlinear interaction between the (0;1) and (1;3) modes.

B. General Three-Dimensional Case

The general form of the solution, Eqs. (40–47), while mathematically exact, is too complicated to enable discerning trends by inspection. Some sample calculations showing various cross sections of the solution surface are presented next. The case of $B = 0.8$, $s = 6$, and $\zeta = 6$ was chosen as the nominal case. This corresponds to a tank of section included angle of 30 deg, and for an outside radius of 10 m has an undisturbed cavity radius of 8 m (i.e., fluid annulus depth of 2 m) and height $10\pi/6 = 5.24$ m.

Calculating the values of the argument λB that satisfy Eq. (47) for the fundamental case $q = m = 0$ [hereafter written as (0;0)] results in an infinite family of eigenvalues with frequencies less than twice the rotation frequency Ω. Figure 5 shows how the highest frequencies of this family change with liquid layer depth, i.e., how the frequencies would vary as the tank is gradually emptied (growing B). The highest frequency (actually a pair of very close frequencies) appears almost unchanged at approximately 1.29Ω. The next highest frequency is different for high and low fill ratios, with a break at $B \approx 0.56$. Similar behavior is observed for the higher harmonics, of which we show the $q = m = 1$ case (1;1). The highest single frequency tends to the spin frequency as the liquid layer tends to zero thickness.

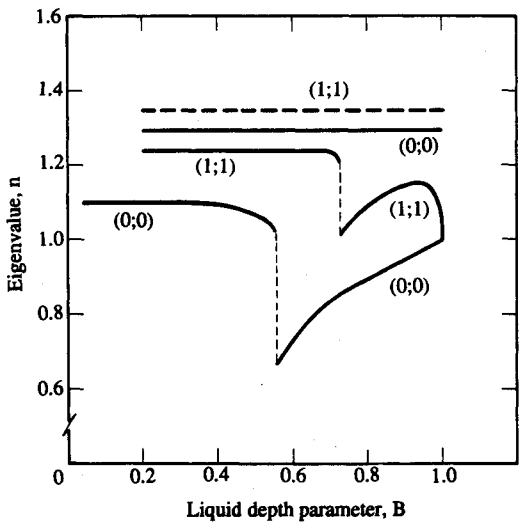

Fig. 5 Highest internal wave frequencies for the fundamental and first equal harmonic, as a function of liquid layer depth; 30-deg sector ($s = 6$); height-to-outer-radius ratio = 0.524 ($\zeta = 6$). Numbers in brackets indicate circumferential and axial harmonics; $n = 1$ is the rotation frequency.

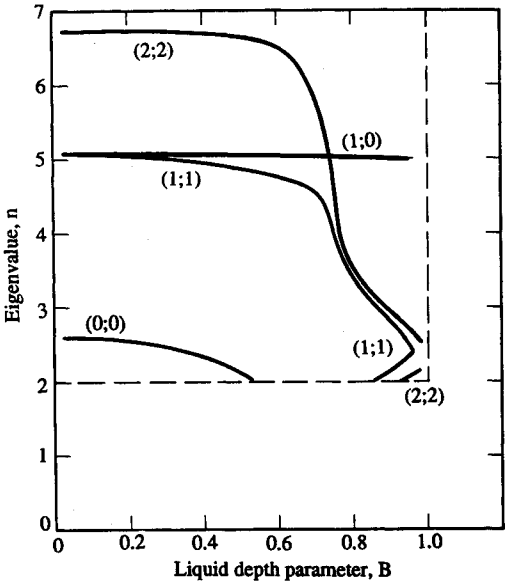

Fig. 6 Sloshing frequencies for the configuration of Fig. 5, as a function of liquid layer depth.

Figure 6 shows the sloshing frequencies expected for the nominal case. The fundamental (0;0) frequency exists only for deep layers, and approaches twice the spinning rate at the value of $B \approx 0.56$ (i.e., where the free-surface radius is approximately equal to the tank height), the same point at which the behavior of the internal wave also changed. This intriguing point, which exists (at different values) for other geometries (s, ζ different), has as yet no physical explanation. Some higher harmonics are also plotted in Fig. 6. A mixed (1;0) harmonic appears at approximately five times the spinning rate for all fill ratios. The (0;1) mode does not occur. The (1;1) harmonic (3/2 wavelengths in both directions) decreases rapidly, for $B \geq 0.7$. For a small, but potentially important, range of radius ratios ($0.86 < B < 0.96$), two sloshing frequencies for the (1;1) mode appear, while for $B > 0.96$, no wave is found. The (2;2) harmonic appears at even higher frequency ($\sim 6.7\Omega$) for deep-liquid layers, while for relatively thin layers, the low-frequency branch appears again. For radius ratios of 0.7–0.8, the (1;1) and (2;2) harmonics are very close, indicating a possibility of resonant interactions and large effects at frequency ranges of 3–4 times the spinning rate.

Each sloshing harmonic has one eigenvalue, except for the thin layer second eigenfrequency for the (1;1) and (2;2) modes, while internal wave eigenvalues appear for a large number of discrete frequencies for each mode, again indicating the expected difference in properties.

Effects of changing the geometry of the tank are examined next. Figure 7 shows the changes in internal wave and sloshing frequencies for tanks of depth $\zeta = 6$ and $B = 0.8$, with varying s (angle between sidewalls). By definition, $s > 0.5$ ($\theta < 360$ deg) and increasing s indicates sidewalls closer to being parallel. The highest internal wave pair of frequencies (marked P) and highest single frequency (F) are shown, both of which decrease slowly with decreasing opening angle (increasing s). (See the discussion of Fig. 5 above, also.)

The higher harmonics for the inertial waves are not shown, to reduce confusion. The harmonics calculated [up to (2;2)] showed similar trends, the value growing slightly with harmonic number. For large s (sidewalls almost parallel) the highest frequencies were all concentrated in the range $0.6 < n < 0.7$, indicating that this is probably a dangerous range. The sloshing frequencies all increase rapidly with s, and all have a limiting value, i.e., they appear only in circular sectors of less than a certain opening angle. Looking at the curves for the (0;0) and (0;1) modes, we see why they did not appear in Fig. 6 for $B = 0.8$. For large s (almost parallel walls)

the only sloshing modes of significance are the (0;0) and (0;1) modes, as the others have extremely high frequencies. For example, the (1;1) mode has a characteristic frequency of 8.75 times the spinning frequency for $s = 16$ ($\Theta = 10$ deg) and $B = 0.8$, and the other modes are even higher.

Figure 8 depicts the modes for a tank of 30-deg sector shape as a function of changing tank heights, for given $B = 0.8$ and 0.5. This case completes the parametric study of tank shapes of Fig. 7. The limit of $\zeta \to 0$ in Fig. 8 is the two-dimensional case described in Sec. IIIA, Eqs. (48-54). The results of Eq. (54) appear as $\times$'s on the ordinate of Fig. 8. We obtain excellent agreement with the curves for the various modes, both for the internal waves (where the two-dimensional model predicts no such modes exist, and the full solution shows that the frequencies of internal modes tend to zero as $\zeta \to 0$) and for the sloshing modes. The full solution, when $\zeta \to 0$, tends to the deep-layer two-dimensional solution [$B \to 0$; Eq. (54)] for each of the harmonics. Obviously, both the (1;0) and (1;1) modes tend to the same value ($n \approx 5.083$) for $\zeta \to 0$, and all other (1;i) modes will tend to the same value.

It is interesting to note that the forms of the curves for decreasing liquid layer depth (growing B) for given geometry (Fig. 6) are qualitatively similar to the functional form of the modes for given layer depth and decreasing tank height (growing ζ). This is a result of the fact that for $n > 2$, the Bessel's functions in Eq. (46) have imaginary arguments and so are calculated as modified Bessel's functions (MBF). Modified Bessel's functions of the second kind, and larger order and argument (>2), have much smaller numerical values than MBFs of the first kind of equal order and argument. Inspection of Eq. (46) shows that the arguments of the Bessel's functions are λB, except in the ratio A_2/A_1 [see Eq. (42) for the explicit form of this expression]. The ratio A_2/A_1 appears only in products with Bessel's functions of the second kind, so that as a result of the argument above, has negligible effect. The argument determining eigenvalues of Eq. (46) is therefore λB; that is, when λB is constant, we approximately obtain the same eigenvalue for high-frequency sloshing. This points out a previously unknown relationship as a kind of similarity parameter, i.e., the ratio of nondimensional tank height to nondimensional liquid layer depth. Further examination of the full significance of this parameter and its possibilities as a predictive tool will be reported separately.

The (0;0) fundamental sloshing mode only appears for tanks of height of more than the free-surface radius (see also Fig. 6), with frequencies close to the critical. The critical frequency of 2Ω is obtained at the limit when the tank height is equal to the free-surface distance from the axis of rotation. This means that as a given tank is emptied, the fundamental sloshing frequency will first decrease and then vanish. The

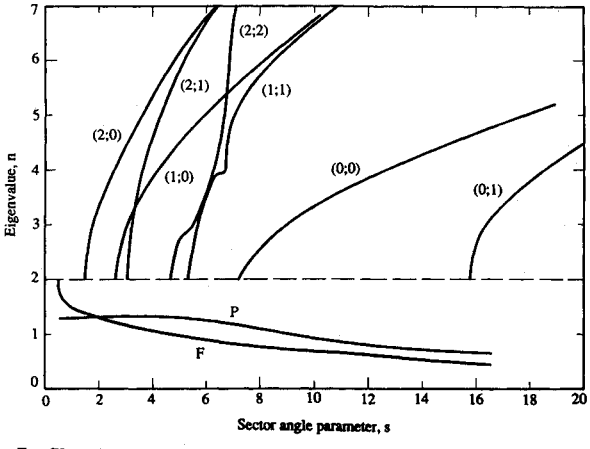

Fig. 7 Sloshing and highest internal wave frequencies as a function of sector angle for $B = 0.8$ and height-to-outer-radius ratio of 0.524. Internal waves are the highest frequency pair (P) and single frequency (F) for the (0;0) mode.

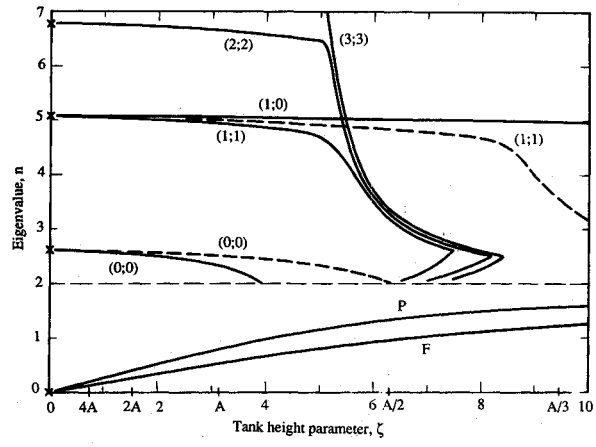

Fig. 8 Sloshing and highest fundamental internal wave frequencies as a function of height parameter ζ for a 30-deg sector tank. Two-dimensional solutions are marked as "$\times$." Full lines are for $B = 0.8$, and broken lines are for $B = 0.5$.

frequency is lower for shorter tanks, this being true also of the higher "equal" harmonics (those with the same number of wavelengths over the free surface in the two orthogonal directions) calculated. The higher harmonics all tend to the deep-layer two-dimensional solution, and are close to that value for all tanks higher than 60% of the outside radius (for the fill ratio $B = 0.8$, depicted). Other fill ratios show similar results, with less full tanks (more shallow liquid layers) having the change in frequency for shorter tanks, as mentioned above.

An interesting observation, paralleling Fig. 6, is the appearance of a second branch of sloshing frequencies for the higher equal harmonics. At a certain tank height, the two frequencies merge, and both do not appear for shorter tanks. Numerical experimentation shows that the relation $\zeta B = \text{const}$ describes this "breakoff" point, with a different constant for each mode. This, again, is a consequence of the relative numerical values of MBFs of first and second kind, mentioned above. The frequency at which the merging occurs is slightly less than the (0;0) two-dimensional frequency and is lower for higher modes.

IV. Concluding Remarks

Some previous studies[1,2,5] indicated that free-surface motions with $n > 2$ could be treated approximately as a nonspinning slosh motion[3] having an effective gravity equal to the average centrifugal acceleration. Figure 6 shows that this supposition is not always true. As the liquid depth decreases ($B \to 1$), the frequency of the $n > 2$ motions at first decreases, as one would anticipate for a nonspinning slosh motion, but then the motion disappears at the point where the frequency would cross the $n = 2$ line. Figure 7 shows a similar behavior when the tank width increases for a fixed depth.

The general nonaxisymmetric case provides a rich variety of wave motions: internal waves with frequencies less than twice the spinning frequency, and sloshing waves of various kinds with frequencies higher than twice the spinning frequency. In certain cases, multiple solutions for a given sloshing harmonic were found, while other combinations of geometrical parameters do not permit any such characteristic frequencies for a given harmonic. The physical significance of many of these predictions is not yet clear, and probably will require experimentation to distinguish the dominant modes.

References

[1]Zedd, M. F., and Dodge, F. T., "Energy Dissipation of Liquids in Nutating Spherical Tanks Measured in a Forced Motion-Spin Table," AIAA Paper 84-1842, Aug. 1984.

[2]Garg, S. C., Furomoto, N., and Vanyo, J. P., "Spacecraft Nutational Instability Prediction by Energy-Dissipation Measurements," *Journal of Guidance, Control, and Dynamics*, Vol. 9, No. 3, 1986, pp. 357-362.

[3]Dodge, F. T., "Empirical Mechanical Model of Propellant Dynamics for a Spinning Spherical Tank with Comparison to Naval Research Laboratory Test Data," *Dynamics Effects of Liquids on Spacecraft Attitude Control, Proceedings of the First INTELSAT/ESA Symposium,* INTELSAT, Washington, DC, April 1984, pp. 19–38.

[4]Agrawal, B. N., "An Overview of INTELSAT Activities on Liquid Slosh," *Dynamics Effects of Liquids on Spacecraft Attitude Control, Proceedings of the First INTELSAT/ESA Symposium,* INTELSAT, Washington, DC, April 1984, pp. 99–120.

[5]Slabinski, V. J., "INTELSAT IV In-Orbit Liquid Slosh Tests and Problems in the Theoretical Analysis of the Data," *COMSAT Technical Review,* Vol. 8, No. 1, 1978, pp. 1–39.

[6]Stewartson, K., "On the Stability of a Spinning Top Containing Liquid," *Journal of Fluid Mechanics,* Vol. 5, Pt. 4, 1959, pp. 577–592.

[7]Stewartson, K., and Roberts, P. H., "On the Motion of a Liquid in a Spheroidal Cavity of a Precessing Rigid Body," *Journal of Fluid Mechanics,* Vol. 17, Pt. 1, 1963, pp. 1–20.

[8]Pfeiffer, F., "Ein Näherungsverfahren für Flüssigkeitgefüllte Kreisel," *Ingenieur-Archiv,* Vol. 43, No. 5, 1974, pp. 306–316.

[9]El-Raheb, M., and Wagner, P., "Vibration of a Liquid with a Free Surface in a Spinning Spherical Tank," *Journal of Sound and Vibration,* Vol. 76, No. 1, 1981, pp. 83–93.

[10]Smedley, G., "Preliminary Drop-Tower Experiments on Liquid–Interface Geometry in Partially Filled Containers at Zero Gravity," *Experiments in Fluids,* Vol. 8, No. 6, 1990, pp. 312–318.

[11]Scott, W. E., "Anomalous Frequency Spectrum of Inertial Waves in a Finite, Rotating Sectored Cylinder," *Physics of Fluids,* Vol. 25, No. 11, 1982, pp. 1944–1948.

[12]Homicz, G. F., and Gerber, N., "Numerical Model for Fluid Spin-Up from Rest in a Partially Filled Cylinder," *Journal of Fluids Engineering,* Vol. 109, No. 2, 1987, pp. 195–197.

[13]Yih, C. S., *Fluid Mechanics,* McGraw-Hill, New York, 1969, pp. 52–55.

[14]Abramowitz, M., and Stegun, I. A., *Handbook of Mathematical Functions,* NBS, Washington, DC, 1964, p. 1046.

James E. Daywitt
Associate Editor